Smart Agricultural Technology 12 (2025) 101323

Contents lists available at ScienceDirect

Smart Agricultural Technology

journal homepage: www.journals.elsevier.com/smart-agricultural-technology

Fraction cover estimation using drone-based multispectral images in six olive cultivars and different planting systems: a case study in Sicily

Eliseo Roma, Santo Orlando *, Alessandro Carella, Riccardo Lo Bianco, Roberto Massenti, Pietro Catania

Department of Agricultural, Food and Forest Sciences (SAAF), University of Palermo, Viale delle Scienze ed. 4, Palermo 90128, Italy

ARTICLE INFO

Keywords:
NDVI
Olive orchard
Precision farming
Spectral mixing analysis

ABSTRACT

Multispectral remote sensing in the olive orchard is expanding, with the aim of improving management for environmental sustainability as well as plant quality and yield. However, the olive tree has a discontinuous vegetative surface, depending on the planting system and cultivar. The aim of this study was to estimate the fraction cover (Fc) with different methods, characterizing the geometric and spectral features of six olive cultivars in four different planting systems. The multispectral data were acquired using a drone equipped with a multispectral camera at 70 m a.g.l. between 12:00 and 13:00 under full sun lighting conditions. Canopy area (CA) and pure Normalized Difference Vegetation Index (NDVI) of canopy and soil were extracted from Geographic Object-Based Image Analysis (GEOBIA). Fc was estimated using two methods: relative vegetation abundance (RA) algorithms and geometric ratio between canopy and available area allotted to each plant according to planting system. In the RA methods, upper (pure canopy NDVI, NDVIc) and lower (pure soil NDVI, NDVIs) limits were obtained from higher frequency class in the bimodal NDVI curve. It was found that the Fc estimated from RA algorithm and geometric ratio were strongly related (R^2 0.97 ***) suggesting that it is a reliable approach, without performing complex image analysis with segmentation and classification algorithms. The proposed model, which integrates NDVI and Fc, provided a tool to assess the health and growth status of olive orchards under various scenarios in order to improve precision management strategies. In addition, it enabled new upper and lower limits useful for the determination of Fc from satellite images.

Introduction

Olive (*Olea europaea* L.) growing is primarily concentrated in the Mediterranean basin and is increasingly expanding to non-European countries such as Australia, California, and South America [1]. It is cultivated using different cultivars, planting systems, and management practices [2]. Super-high-density (SHD) planting systems are increasingly being adopted due to their high productivity and profitability [3]. To implement SHD systems, cultivars with reduced vegetative growth are used to minimize canopy management and promote a balanced vegetative and productive cycle [4,5]. Unfortunately, a relatively limited number of cultivars, primarily Arbequina, Arbosana, Lecciana, Oliana and Koroneiki are well suited to this growing system [6–9]. These cultivars are widely utilised due to their medium-low vegetative vigor which allows them to intercept a greater amount of radiant energy. In addition, they exhibit early fruiting, high and consistent yields, and excellent oil quality, traits that are particularly desirable for the successful adaptation of cultivars to super high-density (SHD) planting systems. Another key characteristic of high-performing cultivars in these planting systems is the greater flexibility of productive branches and higher branching density, which facilitate full mechanization during pruning and harvesting. These features also improve the efficiency of mechanical harvesters, reducing the risk of plant damage. In recent years, significant efforts have been made to identify and select local cultivars suitable for SHD systems [4] to preserve and maintain high levels of biodiversity and olive oil uniqueness. Among these, 'Calatina' has been identified in Sicily, Italy [10].

Knowledge of the main vegetative, productive, and spectral parameters in different farming systems and environmental contexts is a key aspect to increase resource use efficiency [11–13]. Spatially variable application can help increase plant productivity and olive oil quality [14]. Moreover, precise understanding of vegetative and spectral

* Corresponding author.
E-mail address: santo.orlando@unipa.it (S. Orlando).

https://doi.org/10.1016/j.atech.2025.101323
Received 6 May 2025; Received in revised form 4 August 2025; Accepted 13 August 2025
Available online 14 August 2025

parameters can contribute to the improvement of models for estimating irrigation requirements [15] or growth and production of individual plants [16,17]. Recent studies demonstrated the effectiveness of drone-based remote sensing for monitoring olive tree growth conditions under different irrigation regimes or nutrient availability [18–21].

The spectral response can be assessed either by analysing specific regions of the electromagnetic spectrum, for example, green and near-infrared (NIR), or by calculating vegetation indices (VI), depending on the type of sensor used [22–24]. Normalized Difference Vegetation Index (NDVI, [25]) is the most important VI used in olive orchards. VIs from high-resolution images are calculated by averaging the pixel-canopy values to obtain an indicative value of the plant's health condition [26,27]. However, the accurate identification of canopies, soil, and shadows remains one of the most widely studied challenges in the literature, as their coexistence within the same scene can cause signal contamination and lead to incorrect crop status assessments when calculating Vis [28]. This issue is particularly relevant when using satellite imagery, where the low spatial resolution often results in mixed pixels containing both vegetation and non-vegetation elements [29].

In tree plants (e.g. olive), this challenges arise from the low percentage of ground cover, which can strongly influence the overall response, as well as from background and shadow effects [30]. Although the issue of mixed pixels persists in low-resolution data, high-resolution drone data allow for easier classification by using advanced segmentation techniques such as artificial neural networks (ANN), hue-, saturation-, and value-based algorithms, unsupervised K-means algorithms, and other techniques [31,32]. Despite the difficulties related to mixed pixels, research continues toward more precise and simplified methods.

The following biometric parameters are generally used to improve the precision management of olive orchards: canopy height (CH), canopy area (CA, [17,33]), canopy volume (CV) [26,27,34], fraction cover (Fc) and Leaf Area Index (LAI) [16,35]. They can be measured using manual procedures characterised by laborious and expensive processes [36]; however, in recent years the use of drones may overcome these limitations [37–39]. The literature shows various methodologies to determine biometric features remotely, using the Digital Elevation Model (DEM) and Digital Terrain Model (DTM) obtained from the photogrammetric process [18,27,40]. Instead, some of these parameters have several problems that compromise their applicability, e.g. LAI requires accurate ground measurements [35], can be affected by NDVI saturation [41–43] and often cannot be transferred to other conditions [44]. Considering these limitations, there is a tendency to use parameters closely related to crop growth and yield [45].

In recent years, the concept of Fc has been proposed as a robust health index and a potential solution to the above limitations [46,47]. In olive orchards, the Fc enables the quantification of vegetation in a specific area, providing information on growth by monitoring the spectral response [48]. Berry et al. [49] on another hedgerow crop (grapevine), obtained the best variability maps for irrigation management using Fc. Fc refers to the proportion of the land surface covered by a specific vegetation type, in this case, olive tree canopies [48] and it can be calculated from spectral images acquired by drones and/or satellites [46]. High-resolution image analysis techniques that allow for an increasingly precise image segmentation and classification process using Machine Learning (ML) algorithms are generally adopted [50]. In addition, it is possible to split and identify other intermediate-behavior objects that may have a spike effect in the spectral response, such as shadow [28,51]. However, the latter methodology involves long time and specific knowledge for image analysis [31,32]. From satellite images, the spectral mixing analysis (SMA) is one of the most widely used methods to overcome the low resolution limit [52]. This method uses the relative vegetation abundance (RA) algorithms scaled by the maximum and minimum values of the vegetation index [53], allowing to overcome the limitation given from drone image processing. Leolini et al. [48] estimated the Fc in an olive orchard through different indices and found that NDVI is very robust and accurate in determining this parameter. RA algorithms are based on the Beer-Lambert law, with the assumption that a pixel consists of a mixture of only two elements: green vegetation and soil [46]. However, when using satellite platforms, challenges remain in determining pure NDVI values of canopy (NDVIc, upper limit) and soil (NDVIs, lower limit) for tree crops due to their low spatial resolution [19,54] and phenological stages [55]. The published approaches to determine NDVIc and NDVIs, in general, can be divided into two categories: traditional approaches that assign a priori fixed value and improved methods in which both values vary according to specific factors, e.g., species and soil types [56]. To our knowledge, there have been no studies on olive trees that have determined the values of NDVIc and NDVIs and the relationships between these limits and field conditions such as cultivar and planting system from high-resolution images. The literature highlights the need to understand what relationships exist between biometric and spectral conditions when various cultivation aspects such as cultivar and planting system change [57].

The aim of this study was to estimate the fraction cover (Fc) with different methods, characterizing the geometric (canopy area and volume) and spectral (NDVI) features of six olive cultivars in four different planting systems, using drone-based multispectral imagery. In addition, this study aimed to improve Fc estimation by defining new olive grove-specific upper and lower NDVI limits derived from spectral mixing analysis of high-resolution images.

Material e method

Experimental site

The trial was carried out in 2023 in a 2.79-ha experimental olive orchard located near Sciacca, in southwestern Sicily (Fig. 1). The orchard included five traditional Sicilian cultivars (Abunara, Calatina, Cerasuola, Nocellara del Belice - hereafter abbreviated as N. Belice -, and Nasitana) and one widely grown international cultivar (Arbequina). The region has a typical Mediterranean climate, characterised by hot, dry summers and mild winters, with an average annual precipitation ranging between 500 and 600 mm. The soil texture consists of 69 % sand, 13 % silt, and 18 % clay, and is therefore classified as sandy loam according to the United States Department of Agriculture (USDA) system. It has a pH of 7.9 and an organic matter content of 1.1 %.

The experimental plot was divided into two main planting system categories: a hedgerow system (central leader and free palmette, T1) and a three-dimensional canopy system (globe and polyconic vase, T2), according to Massenti et al. [58]. Each planting system was further subdivided based on plant spacing; hedgerow systems included two spacing configurations: 6 × 2 m (833 trees ha^{-1}, T1_1) and 6 × 3 m (555 trees ha^{-1}, T1_2). The volumetric systems included wider spacings: 6 × 4 m (416 trees ha^{-1}, T2_1) and 6 × 6 m (277 trees ha^{-1}, T2_2).

Uniform management practices were applied across the entire experimental field to minimize additional sources of variability. Irrigation was provided at a rate of 800 m^3/ha/year, with weekly applications from July to mid-September. Additionally, an nitrogen, phosphorus, and potassium fertilization was carried out during the spring. Irrigation was applied weekly through two self-compensating in-line drippers per plant, each delivering 16 L/h. In detail, plants received 40 mm of water per week, for a total of 571.2 mm throughout the irrigation season (including 51.2 mm of rainfall).

Ground measurements

At the end of the growing season, simultaneously with drone acquisitions, the trunk cross-section area (TCSA, cm^2) was measured to assess tree vigor. TCSA was recorded at 50 cm above ground level across different planting systems on 54 trees belonging to the Abunara, Calatina, and N. Belice cultivars (18 trees per cultivar). On the same trees, canopy height (CH), width, and depth were manually measured to calculate the total CV and the projected CA, following the methodology

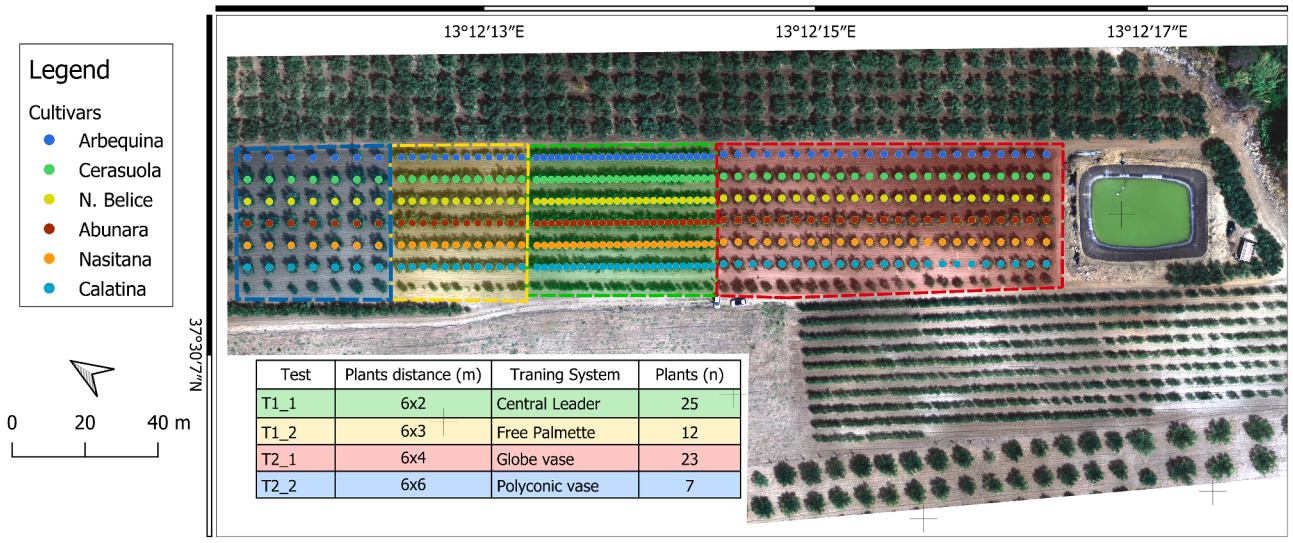

Fig. 1. Experimental area and plot design of the various planting system and cultivar combinations.

used by Massenti et al. [58].

Remote sensing

The drone survey was performed on September 19th using the DJI Phantom 4 (DJI, Shenzhen, China), equipped with a multispectral camera. The multispectral camera was equipped with six spectral bands with centres at 450, 560, 650, 730 and 840 nm coinciding with the Blue, Green, Red, RedEdge and NIR bands. The spectral resolution was of ± 16 nm for visible bands zone while in the NIR band was ± 26 nm. Before the flight, ten ground control points (GCPs) were evenly distributed across the field and georeferenced using the S70G GNSS receiver (Stonex, Milan, Italy). Additionally, reference reflectance panels were positioned within the acquisition zone and recorded at a nadiral angle under the same lighting conditions as those of the flight to ensure radiometric calibration. Each panel had known reflectance values provided by the manufacturer which were entered into the software to perform the calibration. In order to insert the reflectance values of the individual panels, these were manually identified within the individual images and selected using masks.

The flight was performed at a height of 70 m above ground, resulting in a ground sample distance (GSD) of 3.6 cm per pixel. Data acquisition took place between 12:00 and 13:00 under full sun lighting conditions and low wind speeds. The time of day plays a crucial role in determining the proportion of shadow within the image, which could alter the NDVI values of both the crop and the soil [28,59]. Thus, environmental conditions can cause image distortions, potentially leading to minor inaccuracies in the orthomosaic reconstruction [60]. For these reasons, the flight was conducted under optimal conditions to avoid obtaining inaccurate reflectance values.

The flight was carried out in automatic mode with real-time kinematic (RTK) differential correction. Image acquisition was performed with a 70 % front and side overlap between images. The flight direction was East-West, perpendicular to the row orientation to enhance the final quality of the reconstruction process [40].

Photogrammetric process and geographic object-based image analysis

Multispectral images were processed using the software Agisoft Metashape Professional Edition 1.7.3 [61] to obtain the multispectral orthomosaic and DEM. During the photogrammetric process, the images were radiometrically calibrated using the calibration panel and the brightness sensor on top of the drone. Subsequently, the high-resolution orthomosaic obtained was processed using QGIS software ver. 3.28 "Firenze" [62], to calculate NDVI and extract spectral and geometric information of individual plants. The analysis was performed using Object-Based Image Analysis (OBIA), following the procedure outlined in [33].

The DEM processing was used to generate the DTM and the Crop Surface Model (CSM), allowing the estimation of CH and CV of individual plants. CH was estimated using the 95th percentile of the digital number of CSM, while CV was obtained according to previous literature [18,33]. For each CSM pixel, the volume was calculated by multiplying the area of the pixel by its height value and subtracting the value of 0.5, which represents the average height of the canopy from the ground. The total volume of each canopy was calculated by summing the volumes of all the pixels that made up the individual canopies. The segmentation and classification process to differentiate the canopy from the soil and distinguish individual plants was carried out using a machine learning (ML) algorithm implemented in the Orfeo ToolBox integrated in QGIS software. Once the canopies were isolated, the spectral information of the different bands and the NDVI were extracted for each plant.

Such information was extracted by constructing a sub-plot of size equivalent to the planting distances with the centre positioned at the trunk of each plant (Fig. 2). NDVI of the canopy (NDVIc), soil (NDVIs), shadow (NDVIsh) and the average NDVI of the entire sub-plot (NDVIm, mixed) were obtained using the segmentation masks. According to the aim of this work, the NDVIc and NDVIs were also obtained investigating the frequency histogram of each subplot. Fig. 2 shows the generic representation of objects recurrent for each sub-plot. CA represents the zone covered by olive vegetation after the segmentation and classification process, while the rest of the surface was soil and shadow.

To determine the fraction cover, two different calculation methods were used. The first method is based on determining the geometric ratio between the CA and the available area of each plant according to tree spacings. These ratio express the percentage incidence of the CA on the allotted surface per plant, depending on the planting system.

$$F_e = \frac{CA}{A_{tot}} \quad (1)$$

Where CA is the canopy area, A_{tot} is the available area for each plant based for the growing system. The available areas were: 12 m^2 for T1_1, 18 m^2 for T1_2, 24 m^2 for T2_1, and 36 m^2 for T2_2. This method can also be applied as the percentage ratio between the number of canopy pixels ($n_{pixel\ canopy}$) and the total sub-plot pixels (N_{pixels}).

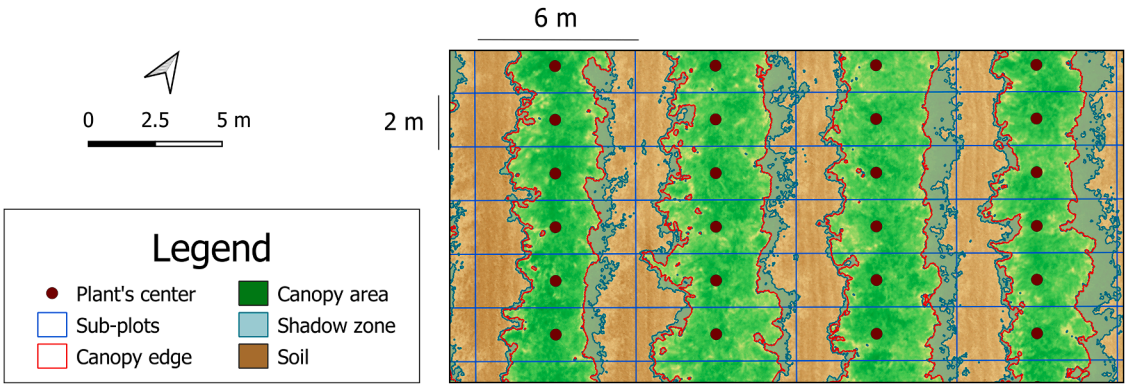

Fig. 2. Schematic representation of canopy area (CA), shadow zone, soil and canopy edge valid for all growing systems in trial.

$$F_e = \frac{n_{pixel\ of\ canopy}}{N_{pixels}} \quad (2)$$

Eqs. (1) and (2) can only be used after applying image segmentation and classification techniques, making the image processing more complex in order to extract information on CA, NDVI, and Fc for individual canopies.

The Linear Spectral Mixture Analysis (LSMA) was the second method for calculating F_c. It is based on the assumption that each pixel contains a linear combination of several "pure" elements (called endmembers) such as green vegetation and bare soil, each with a distinct spectral signature. This approach, also known as the linear NDVI model or the two endmembers model, assumes that there are no significant multiple scattering effects of light between materials and is based on established physical principles such as the Beer-Lambert law [56,63]. This method was applied using the formula proposed by Wittich and Hansing [64] based on the pure NDVI of canopy (NDVIc) and soil (NDVIs) [46]. NDVIc represented the average value of each plant [47,65], while the NDVIs was the value of the average bare soil.

$$F_{c2} == \frac{NDVI_m - NDVI_s}{NDVI_c - NDVI_s} \quad (3)$$

NDVIm was obtained as the mean NDVI value of the entire subplot, while NDVIc and NDVIs were obtained from the classes with a higher frequency in the bimodal NDVI curve in the subplot.

Statistical analysis

Statistical analysis and graphical representations were performed using RStudio 4.4.1 [66] and SigmaPlot ver. 14.0 [67] software. All data obtained for each plant through the image analysis were investigated with a descriptive analysis of the sample. To assess whether Fc varied as a function of the growing system within each cultivar, and to evaluate the combined effect on spectral response, factorial ANOVAs were performed. Before conducting these tests, the normality of the distributions and homogeneity of variances were assessed using the Shapiro–Wilkinson and Levene tests, respectively. Differences among groups were subsequently compared using Tukey's post-hoc test, with a significance level set at $p < 0.05$. Furthermore, coefficient of determination (R^2) and root mean squared error (RMSE) were calculated to evaluate the goodness of fit of the models.

Results and discussion

The acquisition of high-resolution multispectral images from drones and the processed using machine learning algorithms allowed the determination of geometric and spectral parameters of the individual canopies, which were compared between the different cultivars and planting systems. The comparison of the CA and CV of 'Abunara', 'Calatina' and 'Nocellara del Belice' measured on the ground with those estimated by drone shows a R^2 of 0.855 (p-value <0.001) for CA and 0.711(p-value <0.001) for CV (Fig. 3); as observed in other studies [18,68]. In this study, a decrease of estimation accuracy of both parameters was also observed in the less intensive planting systems. This result may be caused by the high percentage of empty spaces compared to the geometric form assumed for the determination of area and volume [33,69].

Plant vigour, expressed as CA, CV and F_c, was more accurately determined in the experiment. Higher vigour was represented by higher values of CA and CV and a subsequent increase in Fc (Fig. 4). Based on CA and CV values, cultivars with the highest vigour were Abunara and N. Belice, with average CA values of 9.5 m^2 and 8.5 m^2 and CV values of 28.2 m^3 and 26.2 m^3, respectively. The varieties with the lowest vigour were Calatina and Arbequina, with CA of 6.8 m^2 and 4.6 m^2 and CV of 18.7 m^3 and 12.1 m^3, respectively.

Concerning Fc, calculated according to Eq. (1), all hedgerow cultivars showed higher values of cover. Specifically, Abunara and N. Belice showed average Fc values of 0.49 and 0.45 while Calatina and Arbequina of 0.34 and 0.25 (Fig. 5). Therefore, cultivar Calatina, compared to the other Sicilian varieties, behaved similarly to the main cultivar used in high-density plantings (cv. Arbequina), confirming what has been observed in previous studies to adopt this cultivar in the SHD system [2,10,57,58]. For each cultivar, the Fc was statistically significant different depending on the planting system (Fig. 5), decreasing from the high-density to low-density. Morales et al. [16] observed that LAI in intensive and super-intensive olive orchards obtained similar results. This suggests that in intensive systems all cultivars can more effectively cover the available space than low-density systems. The planting systems with volumetric shapes (T2) consistently had higher CA and CV values than the hedgerow systems (T1), but opposite behaviour for Fc was observed.

It is evident that the planting system played a crucial role in determining soil cover (Fig. 6). Indeed, CA and Fc were directly related, while the planting system significantly influenced the slope of the relationship. More intensive planting systems tend to reduce the CA per plant while maximizing soil cover, due to the closer spacing and greater canopy continuity along the row. From a physiological perspective, this effect can be attributed to the architectural plasticity of olive trees, which adapt their branching patterns to the available space. In denser systems, trees develop more lateral and compact shoots, increasing canopy closure and light interception efficiency. This structural adaptation enhances the proportion of photosynthetically active tissues relative to woody biomass, facilitating a more efficient use of assimilates for fruiting rather than structural growth [7,9,70]. As a result, even with smaller individual canopy areas, fractional cover values are higher due to the greater continuity and compactness of the canopy along the planting row [2].

Geographic Object-Based Image Analysis (GEOBIA) showed that the simultaneous presence of canopy, soil and shadow pixels in the images

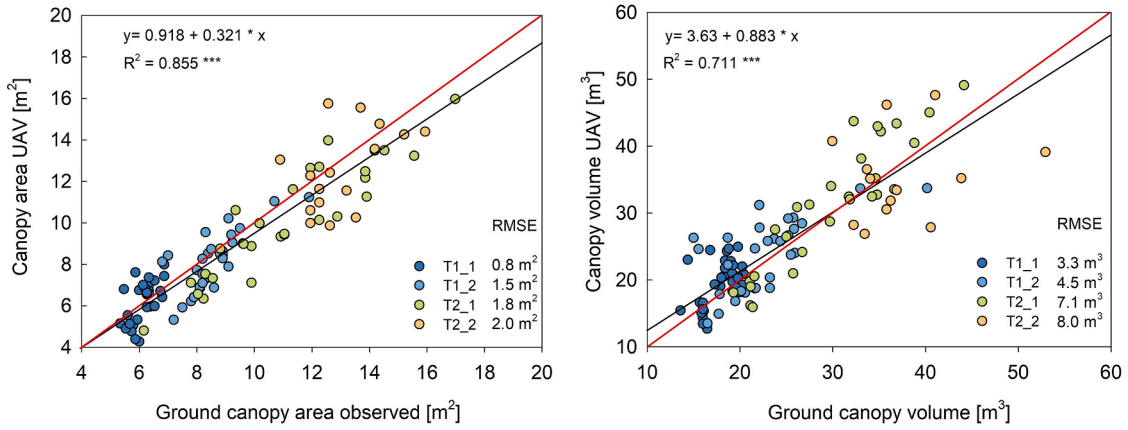

Fig. 3. Comparison of the values for Canopy Area (CA) and Canopy Volume (CV) measured on the ground and estimated by drone. The solid black line represents the linear function, while the red line represents the linear function for $R^2 = 1$. In both graphs, the RMSE (Root Mean Square Error) was evaluated for each planting system. *** p-value < 0.001.

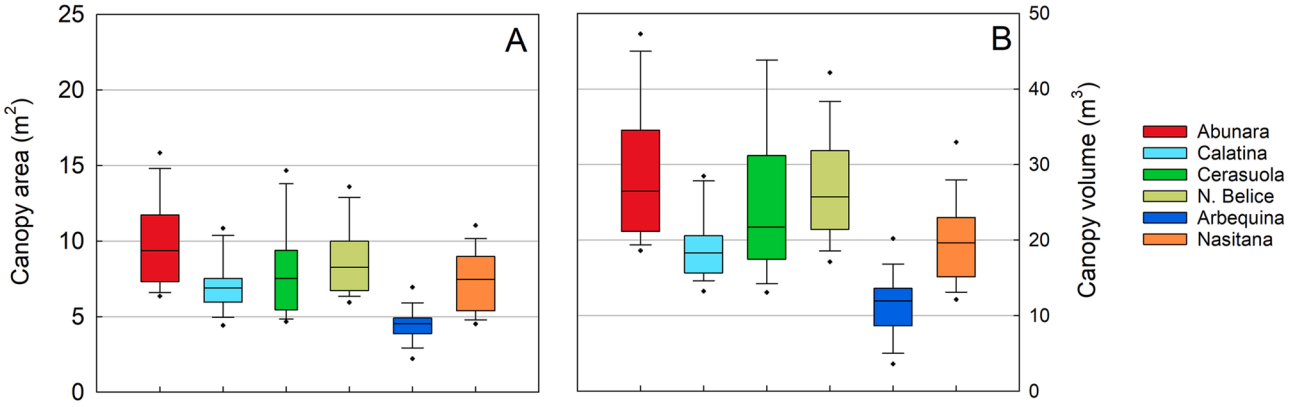

Fig. 4. Drone-estimated Canopy area (A, CA) and canopy volume (B, CV) box-plot of the six cultivars.

results in a non-normalised frequency distribution of DN values in the NDVI map. A bimodal frequency histogram was observed before segmentation and classification, with the two peaks of the curves corresponding to the soil and canopy objects. As can be seen from Fig. 8, there is a difference between the number of canopy, shade or soil pixels depending on the planting system and cultivar. A similar difference was also observed by Coy et al. [71] in herbaceous crops. Inside each sub-plot, the CA covered a surface of 42 % ± 11 % while the shadow and soil were 17 % ± 0.05 and 41 %± 0.12, respectively. Correlation analysis showed that the presence of shade is dependent neither on the canopy nor soil, while the area covered by vegetation and soil were inversely and strictly dependent (Supplementary material 1). In hedgerow systems (T1), the continuity of the canopy results in mixed pixels only along the two exposed sides, whereas in volume forms (T2), these are present along the edge (Fig. 7). Furthermore, in the T2 systems the percentage of canopy was lower than the soil, while the T1 systems showed opposite results, confirming the higher ability of intensive planting systems to cover the available surface.

The results of the Fc obtained by Eq. (3) showed that the RA algorithms were able to effectively estimate the degree of vegetation cover, with a R^2 of 0.968*** between the two methods (Fig. 8). Similarly, de la Casa et al. [72] found a strong relationship between Fc observed and estimated ($R^2 = 0.967$) in soybean. Ding et al. [73], working on maize, reported even high R^2 values ranging from 0.95 to 0.98. These results confirm that the RA method can represent a reliable approach for estimating vegetation cover across different crop types. The results suggest that the RA method could represent a reliable approach for estimating vegetation cover. Moreover, by using the two peaks of the NDVI image frequency distribution, it was possible to accurately determine the minimum and maximum NDVI values [74]. This result could simplify the process of canopy cover estimation, making it independent of increasingly complex OBIA-based analysis processes.

The two-way ANOVA revealed that the values of NDVIm, Fc and NDVIc varied significantly according to planting system, cultivar, and their interaction (Table 1). This effect could have been determined by the different relative frequency of pixel-soil and pixel-canopy within the image [28]. Increasing the degree of coverage (higher Fc) decreased soil pixels allowing an overall increase in NDVIm [75], indeed, the plants with higher NDVIm were those with higher Fc (Fig. 9).

Indirectly, the ANOVA results indicate that each cultivar exhibits distinct vegetative characteristics. As a consequence, LAI-NDVIc or Fc-NDVIc relationship can vary depending on several factors (e.g. species, geographic area). Fig. 9 below shows the hypothetical distribution model of NDVIc and NDVIm as a function of Fc. This model represents the link between NDVI and crop growth. Generally, in herbaceous crops, it occurs at full soil cover and high values of LAI [76], making it unable to determine the actual growth differences of individual plants [44,47]. This model suggests that the olive tree does not reach mean NDVIc values of the entire canopy equal to the saturation level (around 1), despite being a tree plant. This effect could be due to the high percentage of empty spaces and the low leaf density per unit volume of olive trees [16,77]. On the basis of the results seen until now, the training and planting system may influence this process, but a limit will be reached whereby plants will not be able to record increases in NDVIc. An

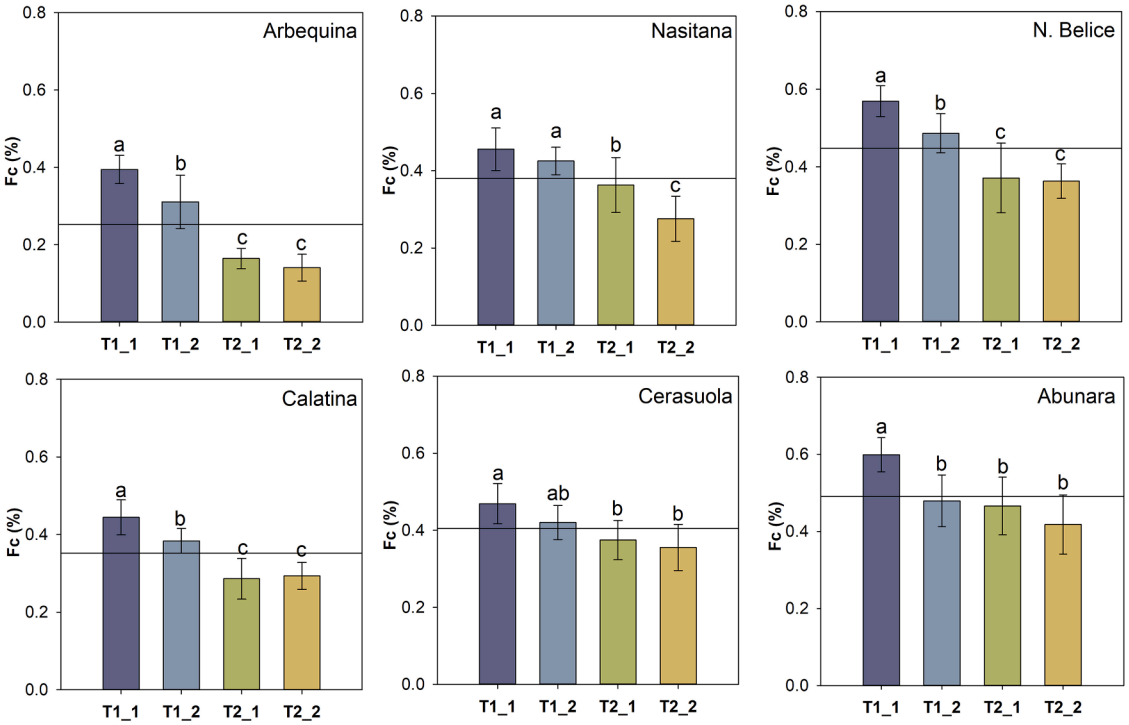

Fig. 5. Fraction cover (Fc) measured by drone for the six cultivars in the planting systems T1_1 (833 plants ha^{-1}), T1_2 (555 plants ha^{-1}), T2_1 (416 plants ha^{-1}), T2_2 (277 plants ha^{-1}). The different letters above the vertical bars (standard deviation) indicate the presence or absence of statistically significant differences obtained through the ANOVA test.

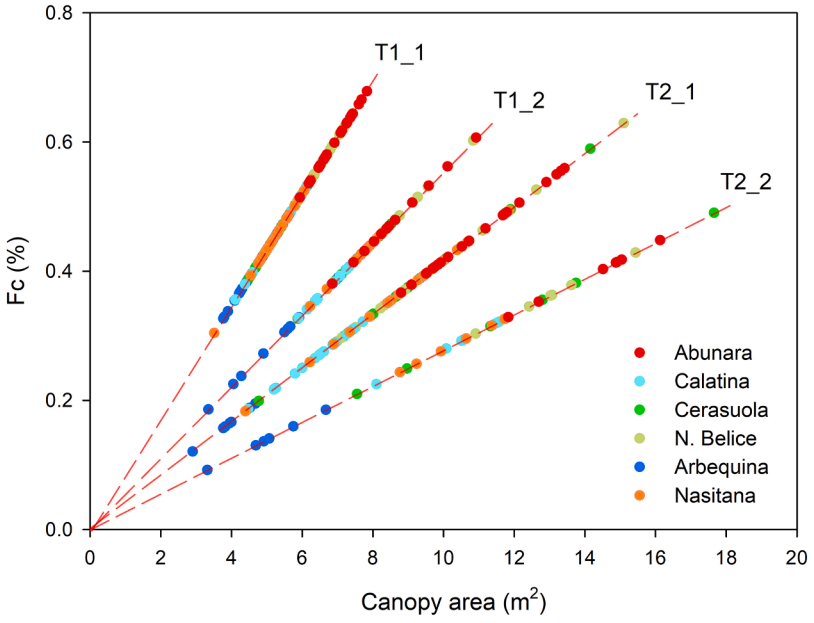

Fig. 6. Relation of CA and Fc of experimental cultivars in the different planting systems: T1_1 (833 p ha^{-1}), T1_2 (555 p ha^{-1}), T2_1 (416 p ha^{-1}), T2_2 (277 p ha^{-1}).

important implication could be observed from the application of Eq. (3) on satellite imagery, as Fc estimates could be improved by using more reliable upper and lower limits. From the results obtained, it can be seen that the NDVIc and NDVIs values correspond to 0.72 and 0.16. NDVIc values variability does not reach saturation problems as generally observed in other crops [46].

Choosing the correct limits can be of fundamental importance for the rapid application of this method. The limits obtained can be used on drone images to obtain an estimate of Fc without adopting advanced segmentation and classification techniques. For satellite applications, the limits obtained will have to be tested in order to be applied on a large scale [19]. However, the selection of these values from the literature is still very difficult and often refers to agronomically incorrect values. Zeng et al. [78] developed a method for calculating the NDVI value corresponding to full green vegetation cover for each land use category using the maximum annual NDVIc value as the NDVI value. Despite its being used, the application of this method on specific crops is not correct as it is not taking into account the real field conditions where herbaceous

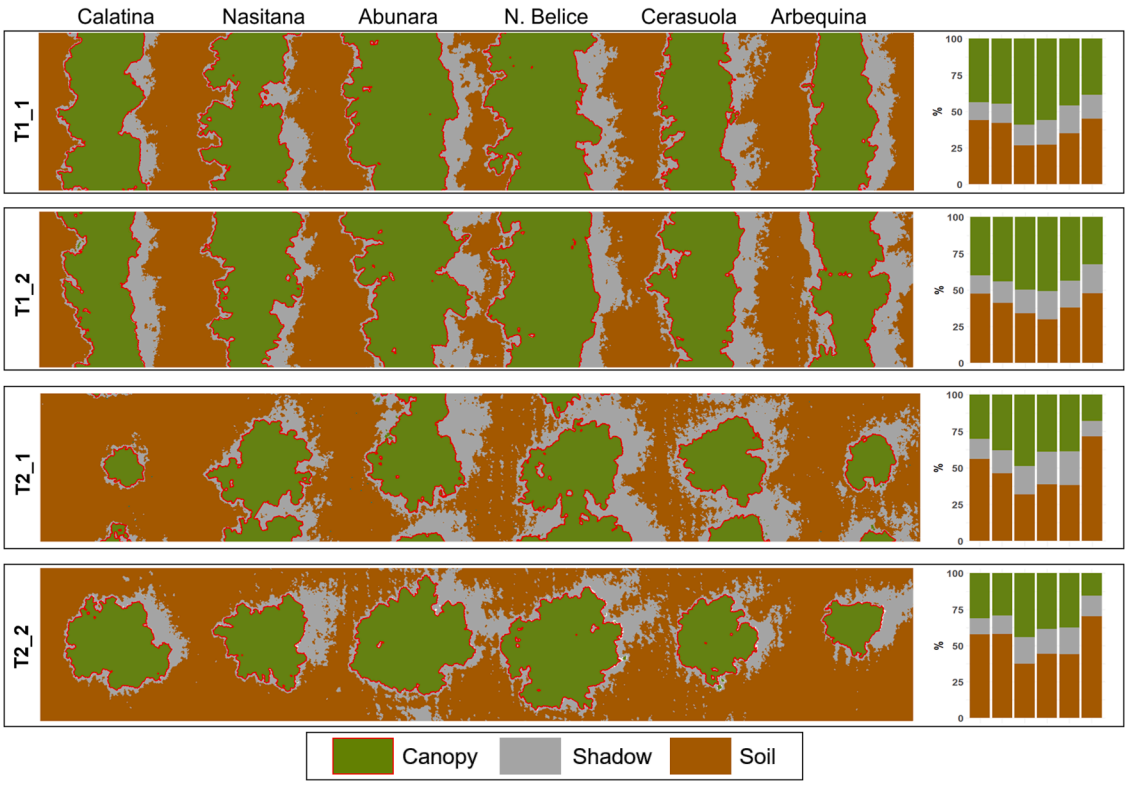

Fig. 7. Representation of canopy, shadow and soil objects detected from the Geographic Object-Based Image Analysis (GEOBIA), among all cultivars (Abunara, Arbequina, Calatina, Cerasuola, Nasitana and N. Belice) and planting systems investigated. Each bar-plot shows the percentage of canopy-shadow-soil average for each cultivar and planting system. Bar-plot follow the cultivars sequence reported above the image.

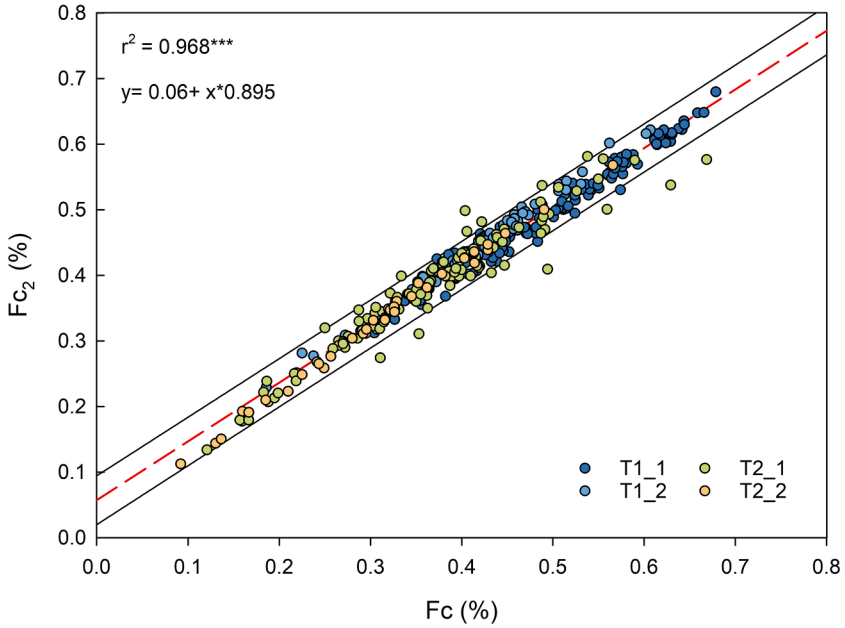

Fig. 8. Linear relationship between the Fc determined by drone and estimated through a relative vegetation abundance model (Fc2). The dashed line represents the linear function, while the solid lines indicate the 95 % confidence levels.

species can alter NDVIc values.

It is the first results that highlight that the NDVIc limit is cultivar specific and not only species [46,56]. In contrast, NDVIs is closely related to soil reflectance, which can change depending on the plot area, especially over large areas. However, NDVIs is usually stable over time and can be obtained by *in situ* measurements, while other authors proposed to use a fixed value (0.05) as a lower limit to estimate the fraction cover, when pure soil NDVI values are not available [47,78]. Since the method used involved extracting the frequency classes of soil and vegetation for each plot, variations in soil reflectance values across different frames did not compromise the Fc estimation. Therefore, the method remains easily applicable even in more complex areas,

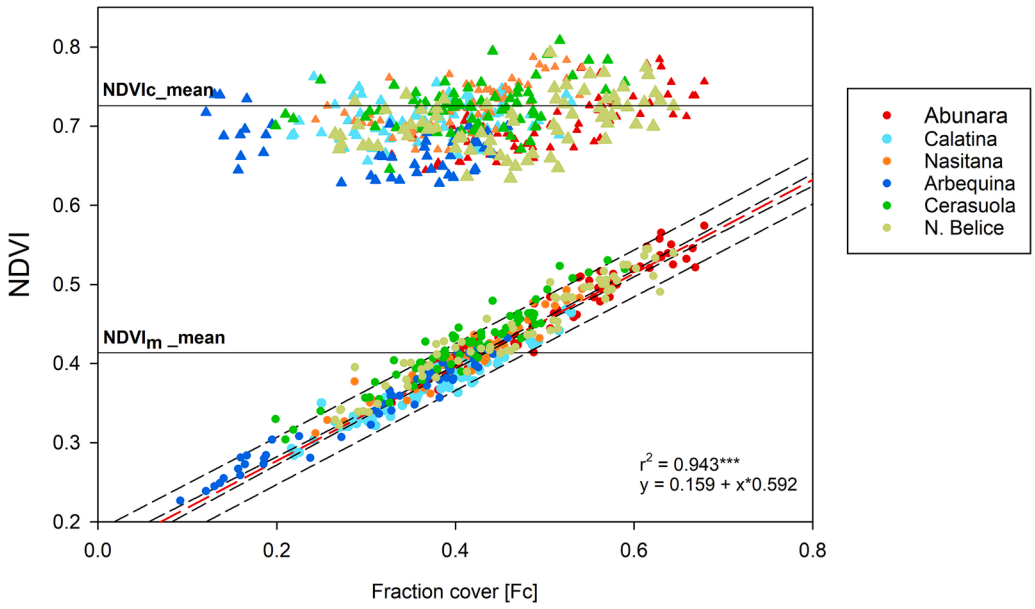

Fig. 9. Scatter plot and linear regression analysis of Normalized Different Vegetation Index of pure canopy (NDVIc) and mixed (NDVIm) values as a function of fraction cover (Fc) of all experimental cultivars. The red dotted line indicates the linear function; the black dashed lines the 99 % and 95 % confidence intervals; the solid black lines the mean values of the whole dataset of NDVIc (0.721) and NDVIm (0.414). The confidence limits are calculated using Fisher-Snedecor F-distribution.

Table 1
two-way ANOVA test results (F values and significant levels) for $NDVI_c$, $NDVI_m$ e F_c. ***($p_{value} < 0.001$), ** ($p_{value} < 0.01$). Test performed for the cultivars (Abunara, Arbequina, Calatina, Cerasuola, N. Belice and Nasitana) and planting system (T1_1, T1_2, T2_1, T2_2).

	Cultivar (C)	Planting system (T)	C x T
$NDVI_m$	92.06**	138.80***	2.85***
F_c	81.86***	151.22***	3.68***
$NDVI_c$	41.22 ***	59.88***	5.49***

overcoming the limitations related to the correct selection of the lower limit value.

NDVIc was found to be sensitive enough different among cultivars [75,79]. Therefore, the results obtained in this study suggest new research perspectives to better investigate how plant vigor may influence NDVIc values. When comparing the measured TCSA values with the canopy spectral response (NDVIc), Fc and NDVIm, the analysisshowed that NDVIm and Fc were significantly related with TCSA ($P < 0.001$, Fig. 10), while NDVIc was not statically related with TCSA ($P > 0.05$).

Linear regression analysis suggested that NDVIm and Fc are good indicators of plant vigor [33,42]. This outcome can be explained since TCSA is a well-established proxy for whole-plant vegetative vigor, parameters such as NDVIm and Fc, which are more directly related to canopy density, reflect more accurately the tree growth dynamics. As observed in other studies, TCSA is not always strictly correlated with the spectral response of plants, despite being a parameter closely related to plant vigor [33]. In fact, TCSA reflects a structural condition formed over years of orchard management, but it does not capture the current, annual growth of the plant. Suboptimal nutrient availability or years with more or less intense pruning may significantly affect the NDVIc values, without causing notable changes in TCSA [38,80]. Some studies have therefore focused on analyzing the annual increment in TCSA, from the beginning to the end of the season, in order to obtain a parameter capable of describing the annual growth trend and thus the actual development of the crop [18,81].

However, other studies have reported strict relationships between

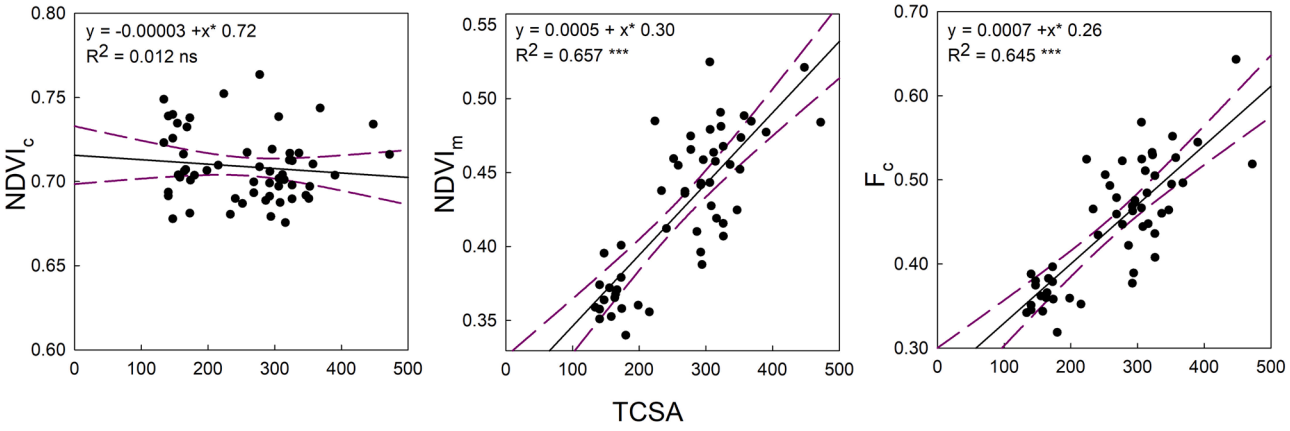

Fig. 10. Linear regression analysis of Trunk Cross Section Area (TCSA) with Normalized Different Vegetation Index of pure canopy (NDVIc), mixed (NDVIm) and Fraction Cover (Fc) determined by drone. The dashed line indicates the linear function and the solid lines the 95 % confidence intervals.

NDVIc and vegetative variables [82,83]. This effect may be linked to the crop and type of crop-data correlated. Indeed, when studying variables closely linked to plant vigor, such as plant productivity or water stress, it is of fundamental importance to know the size of the canopy [49]. Instead, other parameters such as nutrient conditions and chlorophyll content can influence NDVIc or NDVIm if there is an effect on plant vigor [49,84]. In this study, NDVIm and Fc were observed under controlled water and nutrient status, suggesting that both indices can effectively capture differences in growth and vigor among plants, better than the pure NDVIc signal, which is more susceptible to external noise and less tightly linked to tree structural development.

Conclusion

Overall, this study contributes to the state-of-the-art knowledge by demonstrating the effectiveness of high-resolution multispectral imagery acquired via drones for monitoring the spectral variability of olive trees under different planting systems. 'Arbequina' and 'Calatina' showed high adaptability in high-density planting systems, being less vigorous than the other 4 varieties observed. Although cultivar-specific differences in vigour were observed, our results emphasise the importance of considering the interaction between canopy architecture and planting geometry, rather than focusing on cultivar traits alone.

By analyzing pure canopy and mixed pixel (NDVIc, NDVIm), we were able to characterize the spectral behavior of six olive cultivars, highlighting how planting system configuration plays a key role in determining canopy development and fractional cover (Fc). Specifically, more intensive planting systems showed a steeper relationship between CA and Fc, confirming that plant spatial arrangement significantly affects ground cover independently of individual plant size.The use of relative vegetation abundance algorithms made it possible to calculate the canopy area (CA) and Fc of individual plants with high accuracy. These results will simplify and improve the process of determining Fc from high-resolution multispectral drone images without having to perform complex image processing with segmentation and classification algorithms. This approach will also be able to be used on low-resolution satellite images using the upper and lower limits (NDVIc and NDVIs) identified for improved Fc estimation. Finally, the proposed model integrating NDVIc, NDVIm and Fc offers a promising tool for assessing the health and structural growth of olive groves under various scenarios to improve precision management strategies. Although the Fc estimation method used in this study showed very good results, comparable to those derived from image segmentation for the distinction of the various endmembers, it may have some limitations. Among these, the presence of herbaceous species may alter the NDVIm values as well as those of the olive tree and soil, resulting in the overestimation of Fc for the crop using relative abundance models. This can occur because the NDVI signal of the herbaceous ground cover may exceed that of the olive canopy but is not easily discerned. However, most olive growing areas are characterised by semi-arid Mediterranean climates, where the presence of herbaceous ground cover is generally reduced or absent during the leaf and fruit growing season.

Ethics statement

Not applicable: This manuscript does not include human or animal research.

CRediT authorship contribution statement

Eliseo Roma: Writing – original draft, Investigation, Data curation. **Santo Orlando:** Software, Methodology, Investigation, Conceptualization. **Alessandro Carella:** Writing – review & editing. **Riccardo Lo Bianco:** Visualization, Validation. **Roberto Massenti:** Writing – review & editing. **Pietro Catania:** Writing – review & editing, Supervision, Conceptualization.

Declaration of competing interest

The authors declare that they have no known competing financial interests or personal relationships that could have appeared to influence the work reported in this paper.

Acknowledgement

This work was supported by the project "Agritech (MUR, PNRR-M4C2, Investimento 1.4) Università degli Studi di Napoli Federico II, Spoke 2 – Bando a cascata Cod. CN00000022_2 – Università degli Studi di Palermo - Piattaforma digitale per la difesa di precisione dell'oliveto – DIGILOVE – CUP: E63C22000920005.

Supplementary materials

Supplementary material associated with this article can be found, in the online version, at doi:10.1016/j.atech.2025.101323.

Data availability

Data will be made available on request.

References

[1] F. FAOSTAT, Statistics, 2022, Food and Agriculture Organization of the United Nations, Rome, 2022. https://www.fao.org/faostat. accessed 30 April 2025.
[2] R. Lo Bianco, P. Proietti, L. Regni, T. Caruso, Planting systems for modern olive growing: strengths and weaknesses, Agriculture 11 (2021) 494.
[3] J. Tous, A. Romero, J. Hermoso, The Hedgerow System for Olive Growing, 26, Olea (FAO Olive Network), 2007, pp. 20–26.
[4] S. Camposeo, G.A. Vivaldi, C. Montemurro, V. Fanelli, M. Cunill Canal, Lecciana, a new low-vigour olive cultivar suitable for super high density orchards and for nutraceutical EVOO production, Agronomy 11 (2021) 2154.
[5] R. Massenti, A. Ioppolo, G. Veneziani, R. Selvaggini, M. Servili, R. Lo Bianco, T. Caruso, Low tree vigor, free palmette training form, and high planting density increase olive and oil yield efficiency in dry, sloping areas of mediterranean regions, Horticulturae 8 (2022) 817.
[6] L. Rallo, D. Barranco, R. de la Rosa, L. León, Chiquitita'olive, HortScience 43 (2008) 529–531.
[7] A. Rosati, A. Paoletti, S. Caporali, E. Perri, The role of tree architecture in super high density olive orchards, Sci. Hortic. 161 (2013) 24–29.
[8] J. Rufat, A.J. Romero-Aroca, A. Arbonés, J.M. Villar, J.F. Hermoso, M. Pascual, Mechanical harvesting and irrigation strategy responses on 'Arbequina' olive oil quality, HortTechnology 28 (2018) 607–614.
[9] E.M. Lodolini, A. de Iudicibus, P.G. Lucchese, G. Las Casas, B. Torrisi, E. Nicolosi, A. Giuffrida, F. Ferlito, Comparison of canopy architecture of five olive cultivars in a high-density planting system in Sicily, Agriculture 13 (2023) 1612, https://doi.org/10.3390/agriculture13081612.
[10] A. Carella, R. Massenti, G. Milazzo, T. Caruso, R. Lo Bianco, Fruiting, morphology, and architecture of 'arbequina'and 'calatina'olive branches, Horticulturae 8 (2022) 109.
[11] K. Bouhafa, L. Moughli, K. Bouchoufi, A. Douaik, K. Daoui, Nitrogen fertilization of olive orchards under rainfed Mediterranean conditions, Am. J. Exp. Agric. 4 (2014) 890.
[12] D.J. Connor, Towards optimal designs for hedgerow olive orchards, Aust. J. Agric. Res. 57 (2006) 1067–1072.
[13] S.B. Hammami, R. de la Rosa, B. Sghaier-Hammami, L. León, H.F. Rapoport, Reliable and relevant qualitative descriptors for evaluating complex architectural traits in olive progenies, Sci. Hortic. 143 (2012) 157–166.
[14] G. Benelli, G. Caruso, G. Giunti, A. Cuzzola, A. Saba, A. Raffaelli, R. Gucci, Changes in olive oil volatile organic compounds induced by water status and light environment in canopies of Olea europaea L. trees, J. Sci. Food Agric. 95 (2015) 2473–2481.
[15] R.G. Allen, L.S. Pereira, D. Raes, M. Smith, Crop EVAPOTRANSPIRATION-Guidelines for Computing Crop Water Requirements-FAO Irrigation and Drainage Paper 56, 300, FAO, Rome, 1998 D05109.
[16] A. Morales, P.A. Leffelaar, L. Testi, F. Orgaz, F.J. Villalobos, A dynamic model of potential growth of olive (Olea europaea L.) orchards, Eur. J. Agron. 74 (2016) 93–102.
[17] F. Villalobos, L. Testi, J. Hidalgo, M. Pastor, F. Orgaz, Modelling potential growth and yield of olive (Olea europaea L.) canopies, Eur. J. Agron. 24 (2006) 296–303.
[18] G. Caruso, P.J. Zarco-Tejada, V. González-Dugo, M. Moriondo, L. Tozzini, G. Palai, G. Rallo, A. Hornero, J. Primicerio, R. Gucci, High-resolution imagery acquired from an unmanned platform to estimate biophysical and geometrical parameters of olive trees under different irrigation regimes, PLoS ONE 14 (2019) e0210804.
[19] A. Matese, P. Toscano, S.F. Di Gennaro, L. Genesio, F.P. Vaccari, J. Primicerio, C. Belli, A. Zaldei, R. Bianconi, B. Gioli, Intercomparison of UAV, aircraft and

satellite remote sensing platforms for precision viticulture, Remote Sens. 7 (2015) 2971–2990.
[20] E. Roma, V.A. Laudicina, M. Vallone, P. Catania, Application of precision agriculture for the sustainable management of fertilization in olive groves, Agronomy 13 (2023) 324, https://doi.org/10.3390/agronomy13020324.
[21] G. Messina, G. Modica, The role of remote sensing in olive growing farm management: a research outlook from 2000 to the present in the framework of precision agriculture applications, Remote Sens. 14 (2022) 5951.
[22] E. Borgogno-Mondino, A. Lessio, L. Tarricone, V. Novello, L. de Palma, A comparison between multispectral aerial and satellite imagery in precision viticulture, Precis. Agric. 19 (2018) 195–217.
[23] G. Rallo, M. Minacapilli, G. Ciraolo, G. Provenzano, Detecting crop water status in mature olive groves using vegetation spectral measurements, Biosyst. Eng. 128 (2014) 52–68.
[24] G. Messina, G. Modica, Twenty years of remote sensing applications targeting landscape analysis and environmental issues in olive growing: a review, Remote Sens. 14 (2022) 5430.
[25] J.W. Rouse, R.H. Haas, J.A. Schell, D.W. Deering, J.C. Harlan, Monitoring the vernal advancement and retrogradation (green wave effect) of natural vegetation, NASA/GSFC Type III Final Report, Greenbelt, Md 371 (1974).
[26] A.S. Anifantis, S. Camposeo, G.A. Vivaldi, F. Santoro, S. Pascuzzi, Comparison of UAV photogrammetry and 3D modeling techniques with other currently used methods for estimation of the tree row volume of a super-high-density olive orchard, Agriculture 9 (2019) 233.
[27] R.A. Díaz-Varela, R. De la Rosa, L. León, P.J. Zarco-Tejada, High-resolution airborne UAV imagery to assess olive tree crown parameters using 3D photo reconstruction: application in breeding trials, Remote Sens. 7 (2015) 4213–4232.
[28] P.C. Towers, C. Poblete-Echeverría, Effect of the Illumination angle on NDVI data composed of mixed surface values obtained over vertical-shoot-positioned vineyards, Remote Sens. 13 (2021) 855.
[29] P. Zarco-Tejada, G. Sepulcre-Cantó, Remote sensing of vegetation biophysical parameters for detecting stress condition and land cover changes, Estud. La Zona No Saturada Del Suelo VIII (2007) 37–44.
[30] P. Marques, L. Pádua, J.J. Sousa, A. Fernandes-Silva, Advancements in remote sensing imagery applications for precision management in olive growing: a systematic review, Remote Sens. 16 (2024) 1324.
[31] G. Modica, G. De Luca, G. Messina, S. Praticò, Comparison and assessment of different object-based classifications using machine learning algorithms and UAVs multispectral imagery: a case study in a citrus orchard and an onion crop, Eur. J. Remote Sens. 54 (2021) 431–460.
[32] A. Šiljeg, R. Marinović, F. Domazetović, M. Jurišić, I. Marić, L. Panđa, D. Radočaj, R. Milošević, GEOBIA and vegetation indices in extracting olive tree canopies based on very high-resolution UAV multispectral imagery, Appl. Sci. 13 (2023) 739.
[33] P. Catania, E. Roma, S. Orlando, M. Vallone, Evaluation of multispectral data acquired from UAV platform in olive orchard, Horticulturae 9 (2023) 133.
[34] F.M. Jiménez-Brenes, F. López-Granados, A. De Castro, J. Torres-Sánchez, N. Serrano, J. Peña, Quantifying pruning impacts on olive tree architecture and annual canopy growth by using UAV-based 3D modelling, Plant Methods 13 (2017) 1–15.
[35] H. Fang, F. Baret, S. Plummer, G. Schaepman-Strub, An overview of global leaf area index (LAI): methods, products, validation, and applications, Rev. Geophys. 57 (2019) 739–799.
[36] J. Rosell, R. Sanz, A review of methods and applications of the geometric characterization of tree crops in agricultural activities, Comput. Electron. Agric. 81 (2012) 124–141.
[37] J. Berni, P. Zarco-Tejada, G. Sepulcre-Cantó, E. Fereres, F. Villalobos, Mapping canopy conductance and CWSI in olive orchards using high resolution thermal remote sensing imagery, Remote Sens. Environ. 113 (2009) 2380–2388.
[38] J. Estornell, L. Ruiz, B. Velázquez-Martí, I. López-Cortés, D. Salazar, A. Fernández-Sarría, Estimation of pruning biomass of olive trees using airborne discrete-return LiDAR data, Biomass Bioenergy 81 (2015) 315–321.
[39] G. Yang, J. Liu, C. Zhao, Z. Li, Y. Huang, H. Yu, B. Xu, X. Yang, D. Zhu, X. Zhang, Unmanned aerial vehicle remote sensing for field-based crop phenotyping: current status and perspectives, Front. Plant Sci. 8 (2017) 1111.
[40] P. Catania, M.V. Ferro, E. Roma, S. Orlando, M. Vallone, Evaluation of Different Flight Courses with UAV in Vineyard, Springer, 2022, pp. 457–467, https://doi.org/10.1007/978-3-031-30329-6_47.
[41] T.N. Carlson, D.A. Ripley, On the relation between NDVI, fractional vegetation cover, and leaf area index, Remote Sens. Environ. 62 (1997) 241–252.
[42] G. Caruso, G. Palai, L. Tozzini, C. D'Onofrio, R. Gucci, The role of LAI and leaf chlorophyll on NDVI estimated by UAV in grapevine canopies, Sci. Hortic. 322 (2023) 112398.
[43] C.W. Tan, P.P. Zhang, X.X. Zhou, Z.X. Wang, Z.Q. Xu, W. Mao, W.X. Li, Z.Y. Huo, W.S. Guo, F. Yun, Quantitative monitoring of leaf area index in wheat of different plant types by integrating NDVI and Beer-Lambert law, Sci. Rep. 10 (2020) 929.
[44] S. Bajocco, F. Ginaldi, F. Savian, D. Morelli, M. Scaglione, D. Fanchini, E. Raparelli, S.U.M. Bregaglio, On the use of NDVI to estimate LAI in field crops: implementing a conversion equation library, Remote Sens. 14 (2022) 3554.
[45] D.C. Nielsen, J.J. Miceli-Garcia, D.J. Lyon, Canopy cover and leaf area index relationships for wheat, triticale, and corn, Agron. J. 104 (2012) 1569–1573.
[46] L. Gao, X. Wang, B.A. Johnson, Q. Tian, Y. Wang, J. Verrelst, X. Mu, X. Gu, Remote sensing algorithms for estimation of fractional vegetation cover using pure vegetation index values: a review, ISPRS J. Photogramm. Remote Sens. 159 (2020) 364–377.
[47] A.A. Gitelson, Y.J. Kaufman, R. Stark, D. Rundquist, Novel algorithms for remote estimation of vegetation fraction, Remote Sens. Environ. 80 (2002) 76–87.
[48] L. Leolini, M. Moriondo, R. Rossi, E. Bellini, L. Brilli, Á. López-Bernal, J.A. Santos, H. Fraga, M. Bindi, C. Dibari, Use of sentinel-2 derived vegetation indices for estimating fPAR in olive groves, Agronomy 12 (2022) 1540.
[49] A. Berry, M. Vivier, C. Poblete-Echeverría, Evaluation of canopy fraction-based vegetation indices, derived from multispectral UAV imagery, to map water status variability in a commercial vineyard, Irrig. Sci. (2024) 1–19.
[50] M.D. Hossain, D. Chen, Segmentation for Object-Based Image Analysis (OBIA): a review of algorithms and challenges from remote sensing perspective, ISPRS J. Photogramm. Remote Sens. 150 (2019) 115–134.
[51] M. Aboutalebi, A.F. Torres-Rua, W.P. Kustas, H. Nieto, C. Coopmans, M. McKee, Assessment of different methods for shadow detection in high-resolution optical imagery and evaluation of shadow impact on calculation of NDVI, and evapotranspiration, Irrig. Sci. 37 (2019) 407–429.
[52] C.I. Chang, Linear spectral mixture analysis, real-time progressive hyperspectral image processing: endmember finding and anomaly detection (2016) 37–73.
[53] Y. Ding, H. Zhang, K. Zhao, X. Zheng, Investigating the accuracy of vegetation index-based models for estimating the fractional vegetation cover and the effects of varying soil backgrounds using *in situ* measurements and the PROSAIL model, Int. J. Remote Sens. 38 (2017) 4206–4223.
[54] S.F. Di Gennaro, R. Dainelli, A. Palliotti, P. Toscano, A. Matese, Sentinel-2 validation for spatial variability assessment in overhead trellis system viticulture versus UAV and agronomic data, Remote Sens. 11 (2019) 2573.
[55] A. Khaliq, L. Comba, A. Biglia, D. Ricauda Aimonino, M. Chiaberge, P. Gay, Comparison of satellite and UAV-based multispectral imagery for vineyard variability assessment, Remote Sens. 11 (2019) 436.
[56] K. Imukova, J. Ingwersen, T. Streck, Determining the spatial and temporal dynamics of the green vegetation fraction of croplands using high-resolution RapidEye satellite images, Agric. For. Meteorol. 206 (2015) 113–123.
[57] G. Marino, L. Macaluso, F.P. Marra, L. Ferguson, A. Marchese, G. Campisi, P. Volo, V.A. Laudicina, T. Caruso, Horticultural performance of 23 Sicilian olive genotypes in hedgerow systems: vegetative growth, productive potential and oil quality, Sci. Hortic. 217 (2017) 217–225.
[58] R. Massenti, A. Ioppolo, A. Carella, V. Imperiale, R. Lo Bianco, M. Servili, R. Selvaggini, T. Caruso, Growth, yield and oil quality of adult pedestrian olive orchards grown at four different planting systems, Front. Plant Sci. 15 (2024), https://doi.org/10.3389/fpls.2024.1416548.
[59] D. Stow, C.J. Nichol, T. Wade, J.J. Assmann, G. Simpson, C. Helfter, Illumination geometry and flying height influence surface reflectance and NDVI derived from multispectral UAS imagery, Drones 3 (2019) 55.
[60] U.R. Mogili, B. Deepak, Review on application of drone systems in precision agriculture, Procedia Comput. Sci. 133 (2018) 502–509.
[61] Agisoft Metashape User Manual Professional Edition, Version 2.2 2025. Saint Petersburg, Russia (2025) Available online: https://www.agisoft.com/pdf/metashape-pro_2_2_en.pdf, (Accessed on 30 April 2025).
[62] QGIS Development Team, QGIS Geographic Information System Version 3.28. Open Source Geospatial Foundation, 2024. Avialable online: https://docs.qgis.org/3.28/pdf/it/QGIS-3.28-DesktopUserGuide-it.pdf (Accessed on 30 April 2025).
[63] J. Xiao, A. Moody, A comparison of methods for estimating fractional green vegetation cover within a desert-to-upland transition zone in central New Mexico, USA, Remote Sens. Environ. 98 (2005) 237–250.
[64] K. Wittich, O. Hansing, Area-averaged vegetative cover fraction estimated from satellite data, Int. J. Biometeorol. 38 (1995) 209–215.
[65] A.A. Gitelson, A. Viña, T.J. Arkebauer, D.C. Rundquist, G. Keydan, B. Leavitt, Remote estimation of leaf area index and green leaf biomass in maize canopies, Geophys. Res. Lett. 30 (2003).
[66] RStudio Team, Integrated Development for R, RStudio, Inc, Boston U.S., 2019. Available online: http://www.rstudio.com/ (Accessed on 30 April 2025).
[67] Systat Software Inc., SigmaPlot, Version 14.0, User Manual, San Jose, California, US, (2013).
[68] J. Torres-Sánchez, F. López-Granados, N. Serrano, O. Arquero, J.M. Peña, High-throughput 3-D monitoring of agricultural-tree plantations with unmanned aerial vehicle (UAV) technology, PLoS ONE 10 (2015) e0130479.
[69] A. Vinci, R. Brigante, C. Traini, D. Farinelli, Geometrical characterization of hazelnut trees in an intensive orchard by an unmanned aerial vehicle (UAV) for precision agriculture applications, Remote Sens. 15 (2023) 541.
[70] A. Rosati, A. Paoletti, E.M. Lodolini, F. Famiani, Cultivar ideotype for intensive olive orchards: plant vigor, biomass partitioning, tree architecture and fruiting characteristics, Front. Plant Sci. 15 (2024), https://doi.org/10.3389/fpls.2024.1345182.
[71] A. Coy, D. Rankine, M. Taylor, D.C. Nielsen, J. Cohen, Increasing the accuracy and automation of fractional vegetation cover estimation from digital photographs, Remote Sens. 8 (2016) 474.
[72] A. De la Casa, G. Ovando, L. Bressanini, J. Martínez, G. Díaz, C. Miranda, Soybean crop coverage estimation from NDVI images with different spatial resolution to evaluate yield variability in a plot, ISPRS J. Photogramm. Remote Sens. 146 (2018) 531–547.
[73] Y. Ding, H. Zhang, K. Zhao, X. Zheng, Investigating the accuracy of vegetation index-based models for estimating the fractional vegetation cover and the effects of varying soil backgrounds using *in situ* measurements and the PROSAIL model, Int. J. Remote Sens. 38 (2017) 4206–4223, https://doi.org/10.1080/01431161.2017.1312617.
[74] M. Alkassem, S. Buis, G. Coulouma, F. Jacob, P. Lagacherie, L. Prévot, Estimating soil available water capacity within a Mediterranean vineyard watershed using satellite imagery and crop model inversion, Geoderma 425 (2022) 116081.

[75] G. Avola, S.F. Di Gennaro, C. Cantini, E. Riggi, F. Muratore, C. Tornambè, A. Matese, Remotely sensed vegetation indices to discriminate field-grown olive cultivars, Remote Sens. 11 (2019) 1242.
[76] P.J. Curran, Remote sensing of foliar chemistry, Remote Sens. Environ. 30 (1989) 271–278.
[77] E. Roma, P. Catania, M. Vallone, S. Orlando, Assessing the effectiveness of pruning in an olive orchard using a drone and a multispectral camera: a three-year study, Agronomy 14 (2024) 1023.
[78] X. Zeng, R.E. Dickinson, A. Walker, M. Shaikh, R.S. DeFries, J. Qi, Derivation and evaluation of global 1-km fractional vegetation cover data for land modeling, J. Appl. Meteorol. 39 (2000) 826–839.
[79] L. Gomes, T. Nobre, A. Sousa, F. Rei, N. Guiomar, Hyperspectral reflectance as a basis to discriminate olive varieties–a tool for sustainable crop management, Sustainability 12 (2020) 3059.
[80] J. Rubio-Delgado, C.J. Pérez, M.A. Vega-Rodríguez, Predicting leaf nitrogen content in olive trees using hyperspectral data for precision agriculture, Precis. Agric. 22 (2021) 1–21.
[81] J. Ramírez-Cuesta, M. Martínez-Gimeno, E. Badal, M. Tasa, L. Bonet, J. Pérez-Pérez, UAV-based multispectral and thermal indexes for estimating crop water status and yield on super-high-density olive orchards under deficit irrigation conditions, Precis. Agric. 26 (2025) 1–26.
[82] G. Caruso, G. Palai, F.P. Marra, T. Caruso, High-resolution UAV imagery for field olive (Olea europaea L.) phenotyping, Horticulturae 7 (2021) 258.
[83] M.V. Ferro, P. Catania, D. Miccichè, A. Pisciotta, M. Vallone, S. Orlando, Assessment of vineyard vigour and yield spatio-temporal variability based on UAV high resolution multispectral images, Biosyst. Eng. 231 (2023) 36–56.
[84] A. Carella, R. Massenti, F.P. Marra, P. Catania, E. Roma, R. Lo Bianco, Combining proximal and remote sensing to assess 'Calatina' olive water status, Front. Plant Sci. 15 (2024) 1448656, https://doi.org/10.3389/fpls.2024.1448656.